東京大学 大学院新領域創成科学研究科
基盤科学研究系
先端エネルギー工学専攻

平成 21 年度

修士論文

Application of Laser Absorption Spectroscopy to Plasma Wind Tunnel Measurements and Its Tasks

―プラズマ風洞計測におけるレーザー吸収分光法の応用と課題―

2010 年 2 月提出
指導教員　小紫　公也　教授

086073　**野村　哲史**

Acknowledgements

In my work on the master thesis, not only the members and professors in my laboratory, but also the researchers in JAXA and IRS supported me very kindly. I feel a deep appreciation for all.

First I would like to express my appreciation to my supervisor, Prof. Kimiya Komurasaki. He gave me the advice and supported my thesis. Especially before the conference I could practice hard my presentation thanks to him.

I'm pleased that Prof. Yoshihiro Arakawa gave me the advice with respect to the direction of my research at the laboratory meeting nevertheless he is in the Hongo Campus and I seldom have the opportunity to meet him.

Dr. Georg Herdrich invited me to his research group and I could spend a really precious time there. Dr. Stefan Loehle and Mr. Andreas Knapp supported my experiments very kindly. I express here the appreciation to all of the members in IRS.

And Dr. Kazuhisa Fujita and Dr. Hiroki Takayanagi gave me the experience that I did the experiments at JAXA. I feel thanks to them.

I'm pleased to have a nice atmosphere for the research with good members in my laboratory. Mr. Yamaguchi and Mr. Yamagishi helped my experiments, and Mr. Shimada gave me the advice about the numerical calculation. Including the other members in Hongo Campus, the discussion with them really helped my research to proceed.

And Mr. Tanaka also helped my experiments, especially in the developments of the arc wind tunnels.

Last I express my best appreciation to my family.

Contents

List of Table

List of Figure

List of symbols

c	m/s	speed of light
d	m	cavity length
f_c	Hz	frequency of the vibration
f_L	Hz	frequency of the lase modulation
I_{fitted}		fitted laser intensity
I_t		transmitted laser intensity
I_0		intial laser intensity
k_B	J/K	Boltzmann constant
k_0		wave number
M_{LAS}		Mach number measured by LAS
M_{pitot}		Mach number measured by the pitot probe
m	kg	mass of the measured atom
$\dot{m}$	kg/s	flow rate of the working gas
n		refractive index
n_g	m^{-3}	number density of the ground state atoms
n_{777}	m^{-3}	number density of the 3s5S state
n_{844}	m^{-3}	number density of the 3s3S state
p_{amb}	Pa	ambient pressure
p_{pitot}	Pa	pressure measured by the pitot probe
p_{static}	Pa	static pressre
R		reflectivity of mirror
R_g	J/K/mol	gas constant
T_{pop}	K	population temperature
T_{trans}	K	translational temperature
$t_{\delta\omega}$	s	time the laser takes to sweep $\delta\omega$
u_L	GHz/s	scanning speed of the laser frequency
V	m/s	flow velocity
ΔE_{ij}	eV	difference of the energy levels of the state of i and j
$\Delta\nu_{Db}$	GHz	frequency of the Doppler broadening
$\Delta\nu_{Ds}$	GHz	frequency of the Doppler shift
$\Delta\nu_L$	GHz	range of the laser modulation
$\delta\omega$	GHz	full width at half maximum of the transmitted intensity profile
γ		specific heat ratio
λ	nm	wavelength
ν_0	GHz	absorption frequency

θ_t	incident angle

Chapter 1. Introduction

1.1. Reentry to the Earth

In May 2003 a satellite was launched to an asteroid, Itokawa. The name of the satellite is MUSES-C, which is called Hayabusa [1]. Hayabusa had many accidents during its mission, but it overcame them and will return to the Earth in June 2010. And in JAXA a new sample return mission is being planned as Hayabusa II. It may be said that the sample return mission is now one of the most attractive missions in Japan. During the sample return missions the last challenge for the satellites is the reentry to the Earth. To bring back a precious sample the reentry to the Earth has to be achieved safely.

In the long-term vision which JAXA established in 2005, the development of the technology for the Japan's own manned mission is one of the essential parts. In the manned space mission, it is inevitable to save the vehicle from the aerodynamic heating at the reentry.

Thus the development of the technology for the reentry to the Earth is important for the Japanese space developments.

1.2. Aerodynamic heating at the reentry

The reentry to the planet is one of the most dangerous phases in the mission for the vehicle. This can be said when the accident of Columbia is thought of. At the reentry the speed of the vehicle is over several km/s, so in front of the vehicle the strong shock wave is generated and then behind the shock the gas is heated up to over thousands of degrees Kelvin and the molecules of oxygen and nitrogen are dissociated. And then atomic oxygen and nitrogen is recombined at the surface of the vehicle, heating up the surface of the vehicle. This is a surface catalyst reaction [2]. And the strong emission from the shock layer also heats up the vehicle. This is estimated and evaluated by a collisional-radiative model or spectroscopic methods [3].

1.3. Thermal Protection System (TPS)

To protect the vehicle from such a severe aerodynamic heating, a thermal protection system (TPS) is used. And in the development of TPS, there are some unknown phenomena which have to be understood in detail, like a spallation [4] and caulking [5]. So in order to make such phenomena clear, it is necessary to simulate the reentry condition on the ground.

1.4. Plasma wind tunnels

In order to simulate the reentry condition on the ground for the TPS test, plasma wind tunnels are used. Plasma wind tunnels are classified by the way of the generation of the plasma. Here wind tunnels using discharge plasmas are explained briefly. It should be noted that in addition to the

discharge plasma wind tunnels the laser sustained plasma wind tunnels has been developed recently. This novel plasma wind tunnel is expected to achieve a high pressure operation of active gases, like carbon dioxide for the simulation of the entry to the Venus [6].

1.4.1. Arc heater wind tunnel

Conventionally the heating by the arc discharge is widely used. Also in the field of TPS test, the arc heater wind tunnels were developed. Although they might have a disadvantage of the erosion of the electrode which causes a contamination in the flow, this can achieve a high enthalpy flow and long time operation. Therefore this wind tunnel is the most used for the TPS tests. The arc heater wind tunnels are classified into some types by the construction of the electrode. In this work constrictor type arc heater is used. In JAXA 750 kW segmented type arc heater are using for the TPS test.

1.4.2. Inductively coupled plasma generator

The working gas is injected into the quartz tube and then the gas is inductively heated by the coil around the quartz tube though which a radio frequency current goes. IPG does not have a electrode and can operate with an active gases like oxygen and carbon dioxide unlike the arc heater wind tunnels. In Japan an 110kW IPG was installed at JAXA in 2002.

1.5. Thermo-chemical non-equilibrium flow

The state of the plasma wind tunnel flow is not thermal equilibrium. The state of the flow can not be described by just one temperature. In order to characterize the flow condition in detail for the accurate TPS test it is necessary to know many physical quantities.

1.6. Plasma diagnostics

Generally the measurement of the plasma can be classified into the intrusive methods and non-intrusive methods. Many kinds of plasma diagnostics are listed in [7]. The intrusive method is conventionally used and well established but sometimes disturbs the flow. On the other hand, the non-intrusive method does not disturb. Spectroscopic measurements are the typical non-intrusive methods. The spectroscopic measurement offers the information of the state of atoms and molecules so it consists of very detailed information about the flow. Thus the spectroscopic methods are suitable for the non-equilibrium plasma characterization.

The laser spectroscopy has been developed as with the development of the optical technology. Raman spectroscopy [8] and laser induced fluorescence spectroscopy [9] and laser absorption spectroscopy [10] have been applied to the wind tunnel measurements.

Among the various kinds of spectroscopic measurements laser absorption spectroscopy is preferable. By LAS the translational temperature and number density and flow velocity can be obtained. When the use of diode laser is considered as a light source, the measurement systems are compact and less

equipment than LIF or Raman spectroscopy which utilize the dye laser usually. In this work laser absorption spectroscopy is applied for the wind tunnel measurements

1.7. Laser absorption spectroscopy

Laser absorption spectroscopy has been applied in the many fields, the environmental problems [11], combustion gas measurements [12], trace gas measurements and chemical vapor deposition (CVD) [14]. For the wind tunnel measurements Hanson first applied the LAS in 1999 [15]. In the previous researches of our laboratory the translational temperature, number density and flow velocity of the argon flow and mixture gas flow of argon and oxygen have been measured successfully[16][17]. In this work the methods to measure the other physical quantities are developed combining LAS with the pitot probe measurement and LIF measurement.

1.8. Highly sensitive absorption spectroscopy

The laser absorption spectroscopy is suitable for the characterization of the plasma wind tunnel flows. But in the measurement of the air plasma flow the absorption of the oxygen and nitrogen is not detected. In the air plasma the electron temperature is low due to the energy consumption by the dissociation of nitrogen. So the number density of the excited state atoms is not high enough to detect by LAS. Thus it is necessary to enhance the sensitivity of LAS.

Not only in the air plasma wind tunnel measurements but also in the trace gas measurement or other fields, it was necessary to enhance the sensitivity of LAS. So the methods to enhance the sensitivity are developed in the field of trace gas measurements. In principle the longer the optical path length is, the more sensitivity can be achieved. To lengthen the optical path length the optical cavity is built up using highly reflective mirrors. There are a number of researches about highly sensitive cavity absorption spectroscopy. The history and theory of cavity absorption spectroscopy are well summarized in [18].

1.8.1. History of highly sensitive LAS

In 1988 O'keefe has demonstrated a cavity ring down spectroscopy (CRDS) [19]. At that time a broad band pulsed laser was used as a light source since the building up of the cavity mode structure is undesired. But in order to achieve a spectrally high resolution, in 1994 G. Meijer applied a narrow band (but pulse) laser [20]. But this method causes a mode beating problem [21]. To avoid this problem, a Fourier-transform limited pulse laser was applied [22], [24]. Then in 1997 Romanini applied a CW laser [23], since the application of a CW laser is attractive if the use of a diode laser, which is compact and inexpensive, is considered.

Although the various schemes were developed for the high resolution measurements as mentioned above, their experimental setups are more involved than the traditional CRDS. In 1998, Meijer et al demonstrated a cavity enhanced absorption spectroscopy (CEAS) [25]. And O'Keefe demonstrated an integration cavity output spectroscopy (ICOS) [26]. At both works, the setups are

simple comparing to the CW CRDS.

After 2000, an increasing number of researches were demonstrated and CRDS, CEAS and ICOS are developing. In this work, the application of CEAS is considered.

1.8.2. Tasks for the application of CEAS to the plasma wind tunnels

In the application of CEAS to the plasma wind tunnel measurements there are some tasks for that. The one is the influence of mechanical vibration from a vacuum pump or other experimental facilities to the optical cavity. The optical cavity is very sensitive to the mechanical vibration. Even the vibration which amplitude is order of the laser wavelength disturbs the measurements. The second is the time resolution. In the single pass LAS, the time resolution is decided by the time responsiveness of a photo detector as long as the CW laser is used. But the time resolution of CEAS is decided by the time interval of the each transmitted signals. For some wind tunnel measurements [17], the high time resolution is needed. The last is the demand of the *in situ* measurement. The plasma wind tunnel flow often has a distribution of temperature and density. In the application of the single pass LAS, the Abel inversion is usually applied to obtain the spatially resolved results. But as to CEAS, it is difficult to measure the flow traversing the probe laser.

So the tasks are to yield the vibration influence to the cavity and to achieve a highly time-resolved measurement and spatially resolved measurement. In this work, the mechanical vibration is studied experimentally.

1.9. Objectives

With the aforementioned background in this research the objectives are as follows,

1) Development of the novel measurement by the combination of LAS with the pitot probe measurement

2) Development of the novel measurement by the combination of LAS with LIF

3) Experimental study of the mechanical vibration influence to the optical cavity

Chapter 2. Measurement of the specific heat ratio by the combination of LAS and the pitot probe measurement

2.1. Principle of the specific heat ration estimation

2.1.1. Estimation of Mach number by the pitot probe measurement

The total pressure of the flow p_{pitot} is measured by a pitot probe and from the ratio of p_{pitot} to the static pressure p_{static} Mach number M_{pitot} can be obtained by Eq. (1) (in case of the super sonic flow).

$$\frac{p_{\mathrm{pitot}}}{p_{\mathrm{static}}} = \left[\frac{(\gamma+1)M_{\mathrm{pitot}}{}^2}{2}\right]^{\frac{\gamma}{\gamma-1}} \left[\frac{\gamma+1}{2\gamma M_{\mathrm{pitot}}{}^2-(\gamma-1)}\right]^{\frac{1}{\gamma-1}}. \tag{1}$$

In case of (γ −1)/2 $\gamma \ll M_{\mathrm{pitot}}{}^2$, Eq. (1) can be rewritten as follows,

$$M_{\mathrm{pitot}}{}^{-2}\left(\frac{p_{\mathrm{pitot}}}{p_{\mathrm{static}}}\right) = \left[\frac{\gamma+1}{2}\right]^{\frac{\gamma+1}{\gamma-1}} \gamma^{\frac{1}{\gamma-1}} = f(\gamma). \tag{2}$$

In this work, it is assumed that p_{static} is identical to the ambient pressure p_{amb}, since there is no vertical flow to the flow axis.

2.1.2. Estimation of Mach number by LAS

As described in [7] the translational temperature T_{trans} and flow velocity V can be obtained by following equations,

$$\Delta\nu_{\mathrm{Db}} = \frac{\sqrt{8k_{\mathrm{B}}\ln 2}}{c}\sqrt{\frac{T_{\mathrm{trans}}}{m}}\nu_0, \tag{3}$$

$$V = \frac{c\Delta\nu_{Ds}}{\nu_0\cos\theta}. \tag{4}$$

Here k_{B}, c, m and ν_0 are Boltzmann constant, the speed of light, atomic mass of the measured atoms and the frequency of the absorption. Thus Mach number can be obtained by LAS as follows,

$$M_{\mathrm{LAS}} = \frac{V}{\sqrt{\gamma R_{\mathrm{g}} T_{\mathrm{trans}}}}. \tag{5}$$

Here the gas constant R_{g} is a function of the temperature. But in this work the argon gas is measured. Argon is mono atomic gas so it is assumed that R_{g} is invariant.

2.1.3. Estimation of the specific heat ratio

As explained above, Mach number can be estimated by two independent methods. So by following equation the specific heat ration can be deduced,

$$\frac{f(\gamma)}{\gamma} = \frac{R_{\mathrm{g}}T_{\mathrm{trans}}}{V^2}\frac{p_{\mathrm{pitot}}}{p_{\mathrm{amb}}}. \tag{6}$$

2.2. Experimental setup

2.2.1. Arc heater wind tunnel

The schematic overview of the arc heated wind tunnel used in this work is shown in Fig. 1. The throat diameter is 2 mm and nozzle exit diameter is 30 mm. Table 1 shows the operational conditions of the arc heater wind tunnel. The thermal efficiency is deduced by the measurement of increasing of the temperature of the cooling water. In the nozzle expansion, the flow is totally covered with the boundary layer so at the edge of the flow, the velocity is subsonic.

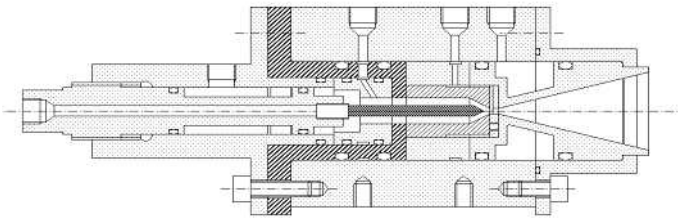

Fig. 1 Schematic overview of the arc heater wind tunnel.

Table 1 Operational conditions of the arc heater.

Parameters	Values
input power, kW	1.2
thermal efficiency	0.39
argon flow rate, slm	4.0
ambient pressure, Pa	34
average specific enthalpy, MJ/kg	3.9

2.2.2. Pitot probe measurement

In our laboratory a miniature pitot probe was manufactured. The photograph of the pitot probe measurement and plasma flow and the schematic of the pitot probe are shown in Fig. 2 and Fig. 3. The probe is made of cupper and cooled by water. The diameter of the probe is only 5 mm that guarantees the highly spatial resolution at the measurement of the flow which diameter is 30 mm. The pressure port is connected to the pressure gauge (F-tron, DIAVAC). And the data was recorded by the oscilloscope (DL708, YOKOGAWA). The probe is traversed the flow by a stepping motor. The measured cross section is 43 mm away from the nozzle exit.

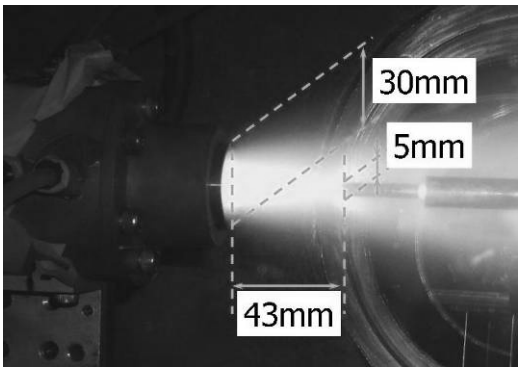

Fig. 2 Photo of the pitot probe measurement in an argon plasma plume.

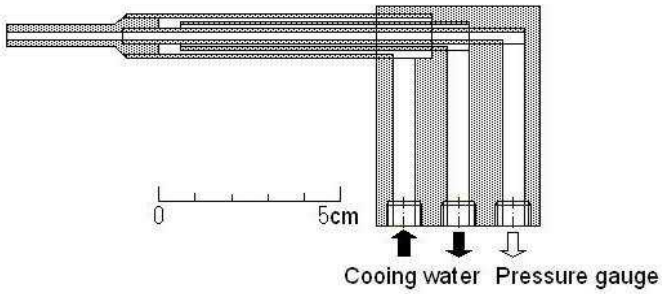

Fig. 3 Schematic of the miniature pitot probe.

2.2.3. Laser absorption spectroscopy

The experimental setup of LAS is almost same as the work in [7]. The target absorption line is 772.42 nm of argon. Fig. 4 shows the picture of the LAS measurement. The measured cross section is 43 mm away from the nozzle exit. This is the same as the measurement by the pitot probe. The angle between the flow axis and laser direction is 73 degree. This angle is obtained by measuring the displacement of the laser position between at the windows of chamber.

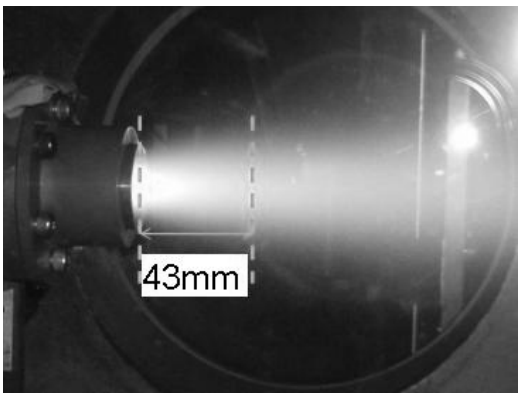

Fig. 4 Photo of the plasma flow to which LAS is applied.

2.3. Result and discussion

2.3.1. Pressure distribution and evaluation of the error of the pitot probe

The distribution of the pitot pressure and Mach number is shown in Fig. 5. The regulation line is the Gaussian fitting by the least square to the six times measurements data. At the edge of the flow the velocity is subsonic as aforementioned. The deviation of the data is very small. The accuracy of the two pressure gauges which are connected to the chamber and the probe is 1 % relatively, so the measurement error of the pressure ratio is estimated as 2 %, summing the two errors.

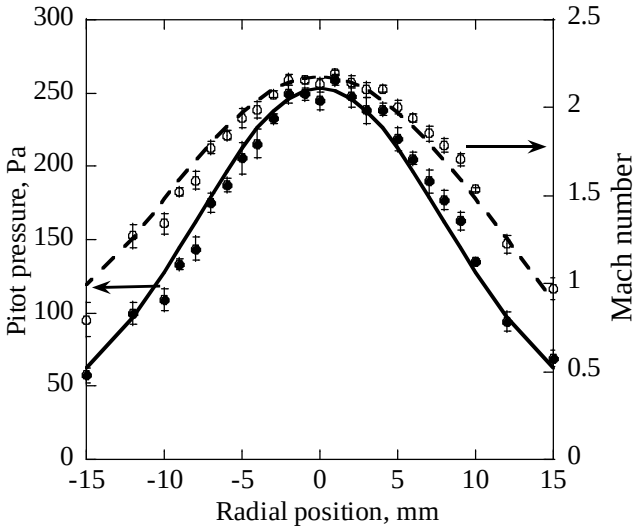

Fig. 5 Radial distributions of p_{pitot} and M_{pitot}, assuming γ is 5/3.

2.3.2. Results and evaluation of the error of LAS

The translational temperature and flow velocity distributions are shown in Fig. 6. The regulation line is the Gaussian fitting by the least square to the three times measurements data. It

took tens of minutes to take the three times data. This causes the relatively large deviation, compared with the pitot probe measurement.

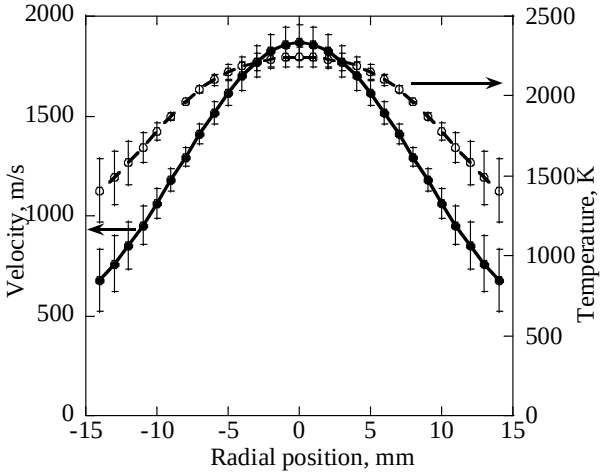

Fig. 6 Radial distributions of V and T_{trans} measured by LAS.

Here the error of LAS is discussed. The velocity of the flow at the center is about 2000 m/s, corresponding to the 2.6 GHz of $\Delta\nu_{\mathrm{Ds}}$. The line width of the probe laser is narrower than 1 MHz. The optical path length is about 1 m. This means the error of the angle estimation is less than 0.3 %. Thus the error of the velocity measurement is negligible (less than 0.1 %). At the evaluation of the error of temperature measurement, the Gaussian fitting error should be taken into account. Since the error of $\Delta\nu_{\mathrm{Db}}$ is negligible as the velocity measurement, the temperature measurement error can be equated as follows [7],

$$\frac{\Delta T_{trans}}{T_{trans}} = \frac{1}{\sqrt{\ln 2}}\left|\frac{\Delta\left(I_{\mathrm{t}}/I_0\right)}{\left(I_{\mathrm{t}}/I_0\right)\ln\left(I_{\mathrm{t}}/I_0\right)}\right|. \tag{7}$$

Here I_{t} and I_0 is transmitted laser intensity and initial intensity of the laser. At the center of the plume, I_{t}/I_0 is about 0.5. In case of $\Delta(I_{\mathrm{t}}/I_0)/(I_{\mathrm{t}}/I_0)$ = 1% $\Delta T_{\mathrm{trans}}/T_{\mathrm{trans}}$ is estimated as 1.7 %. If the absorbance is small and I_{t}/I_0 is 0.9, $\Delta T_{\mathrm{trans}}/T_{\mathrm{trans}}$ is about 11 %.

2.3.3. Evaluation of the error of the estimation of γ

Assuming that γ is 5/3, the distributions of Mach number are obtained as shown in Fig. 8. There is a good agreement between two results. The reason why the deviation of the data around the edge of the flow is larger than that of around center of the flow is mainly the instability of the flow. So in the following discussion the center of the flow is considered. If γ changes from 1 to 3, Mach number changes as shown in Fig. 8. Since M_{LAS} is identical to M_{pitot}, γ can be estimated as 1.30.

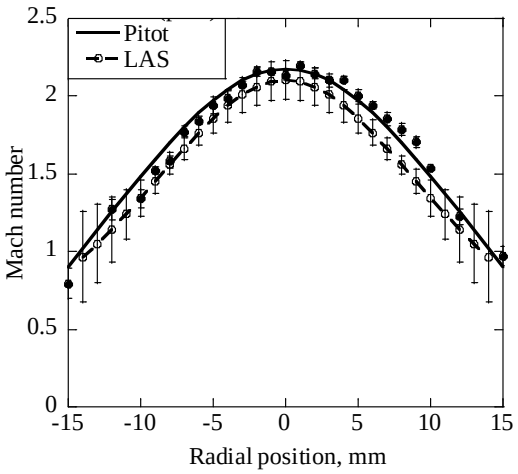

Fig. 7 Radial distributions of M_{LAS} and M_{pitot}, assuming γ = 5/3.

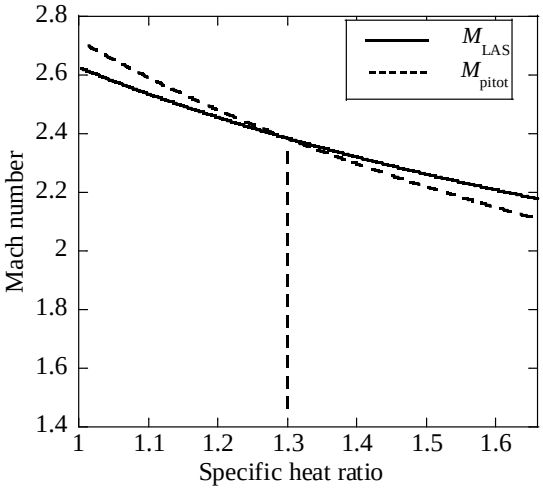

Fig. 8 Mach numbers estimated in LAS and the pitot probe measurement as a function of assumed γ.

By the differential of Eq. (6), the error of γ is equated as

$$\left|\frac{\gamma f(\gamma)'}{f(\gamma)}-1\right|\left|\frac{\Delta\gamma}{\gamma}\right| = \left|\frac{\Delta\left(p_{\mathrm{pitot}}/p_{\mathrm{amb}}\right)}{p_{\mathrm{pitot}}/p_{\mathrm{amb}}}\right| + \left|\frac{\Delta T_{\mathrm{trans}}}{T_{\mathrm{trans}}}\right|. \tag{8}$$

For $\gamma = 1.30$ the accuracy of $|\Delta\gamma/\gamma| = 0.86\times(2\%+1.7\%) = 3.2\%$ is estimated.

2.4. Summary

The laser absorption spectroscopy and pitot probe measurements are applied to Mach number measurements of the arc heater wind tunnel flow of argon. The distribution of Mach number is

obtained and each two results have a good agreement. By the combination of these two independent measurements, the scheme to estimate the specific heat ratio is developed. And by the error analysis, the error is estimated as 3.2%.

Chapter 3. Application of LAS to the quasi stationary inductively coupled heated plasma wind tunnel

Among the grate number of energy levels, the ground state is the most important factor. But the number densities of the atoms in the other energy levels are also important for building of the Collisional-Radiative model and for the evaluation of the wall catalytic phenomena of the TPS test. In this work LAS has been applied to the inductively coupled plasma wind tunnel (IPG3) in the institute of space system in Stuttgart University and the number density of the atomic oxygen in the metastable state is obtained. Then by the combination with the number density measured by the laser induced fluorescence, the population temperature is estimated.

3.1. Inductively coupled plasma wind tunnel

The schematic of the IPG3 which is installed in IRS of Stuttgart University is shown in Fig. 9. The vacuum chamber is 2 m in diameter and 2.5 m in length. The working gas is injected into the quartz tube and heated up by a high frequency current applied to the induction coil around the tube. The exit diameter of the tube is 80 mm.

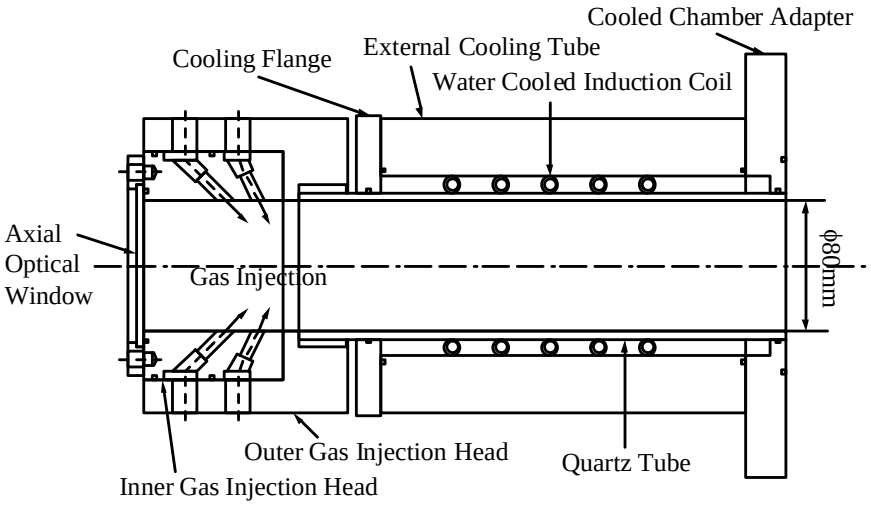

Fig. 9 Schematic of the IPG3.

3.1.1. RF circuit

The schematic of the RF circuit of the IPG3 is depicted in Fig. 10. This is part of a Meissner-type resonant circuit. Its operational frequency can be optimized to achieve a high-energy coupling efficiency for various gas species by switching the number of capacitor [28]. In this work, the operational frequency is 0.73 MHz. Table 2 shows the operational conditions of the IPG3. At the

both of LAS and LIF measurements, the measured plane was 140 mm away from the exit of the generator.

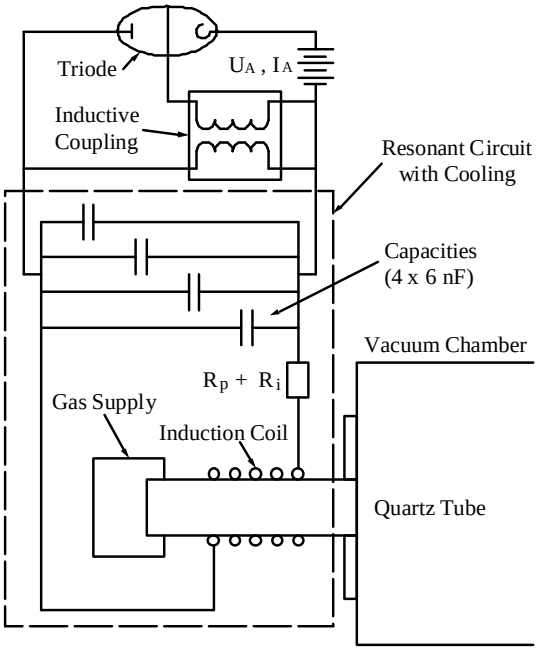

Fig. 10 RF circuit of IPG3.

Table 2 Operational conditions of IPG3.

working gas	O_2
$\dot{m}$	3 g/s
P_A	110 kW
U_A	6000 V
coil turn	5.5
number of capacitors	4
p_{amb}	30 Pa

3.1.2. History of the emission of flow

The flow of the IPG3 is not stationary plasma due to the characteristic of the power supply. There is a ripple at the DC power supply which is rectification of the three-phase and 50 Hz alternating current. The history of the emission from the plasma flow is detected by a photo detector (DET110, Thorlab. Inc.). The result is shown in Fig. 11. The intensity of the emission fluctuates at the frequency of 300 Hz. Thus in the data analysis it is assumed that points of 1 and 9 (which is indicated in Fig. 11) are on the same condition. In the same way, the points of 2, 4, 6 and 8 are the same and the points of 3, 5 and 7 are the same, the points of 10 and 12 are the same.

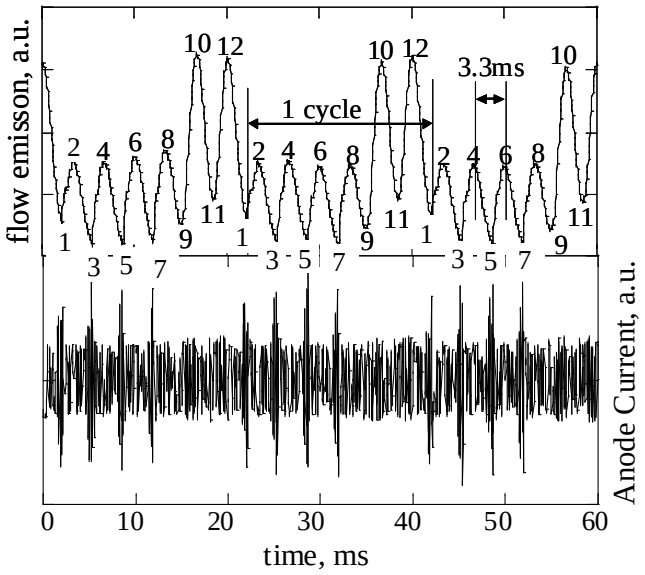

Fig. 11 History of the emission of the flow and anode current.

3.2. Application of the laser induced fluorescence (LIF) to IPG3

In the previous research, LIF has been applied to IPG3 to measure the number density of the ground state atomic oxygen [29]. As a result, the number density and translational temperature was obtained as shown in Table 3.

Table 3 Results of LIF ($\dot{m}$ =3 g/s, p_{amb}=26 Pa, and U_A=6300 V).

n_g	$6 \cdot 10^{20}$ m^{-3}
T_{trans}	3500 K

3.3. Measurement system

The schematic and photograph of the experimental setup of the LAS system is shown in Fig. 12 Fig. 13. A tunable diode laser with external cavity (Velocity Model 6316, New Focus, Inc.) is used as a light source. The laser linewidth is less than 300 kHz. The modulation frequency was set at 1 Hz. The free spectral range of an etalon (Neo Arc) which is used as a wave meter is 1 GHz. The probe beam was introduced to the chamber though the single mode optical fiber and the diameter of the laser is 2mm. The transmitted signal was detected by a photo detector (DET110/M, Thorlab, Inc.) with a band pass filter (FB 840-10, Thorlab, Inc.). The detector was put 3 m away from the flow axis in order to avoid the emission. The data was recorded using a digital oscilloscope (NR-2000, Keyence, Co.) with 14-bit resolution at the sampling rate of 20 kHz. This sampling rate is enough high to follow the oscillation of the plasma flow.

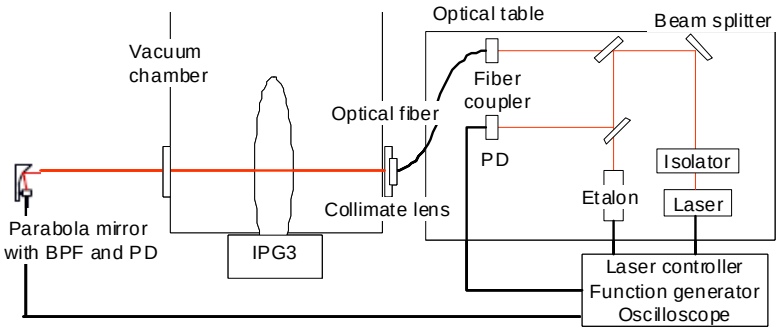

Fig. 12 Schematic of the LAS measurement system.

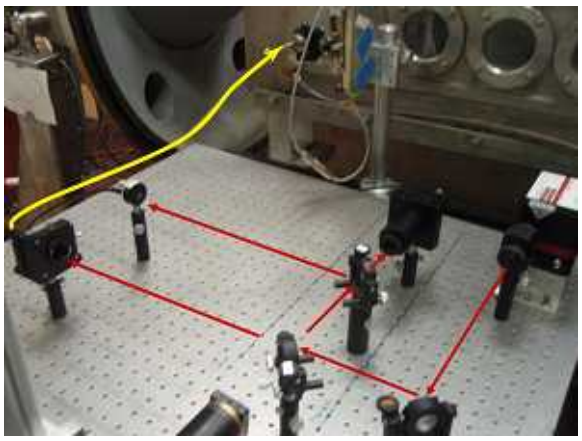

Fig. 13 Photo of the experimental set up of LAS.

3.4. Experimental results

3.4.1. Oscillation of the flow state

A typical absorption profile obtained by LAS for IPG3 is shown in Fig. 14. Fig. 15 is the extended figure of Fig. 14 from 11 GHz to 14 GHz and shows the history of a transmitted laser intensity and absorbance. The signals fluctuate at 300 Hz. Here the oscillation shown in Fig. 15 is the most typical type, so it is assumed that the cycle in Fig. 15 is repeated during the all operation. The signal is different from the previous research in which the other transition of atomic oxygen was measured by LAS [17]. But the input power of IPG3 is the same as that of the previous work, so it can be compared with each other. In this work, local maximum and minimum value are extracted in the each cycle and other points are fitted by a sine curve.

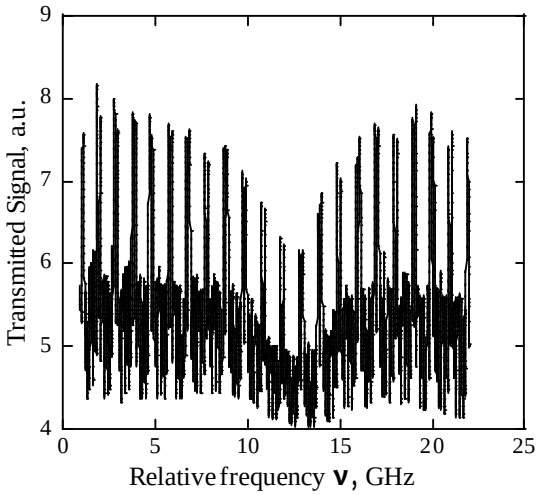

Fig. 14 Typical absorption profile.

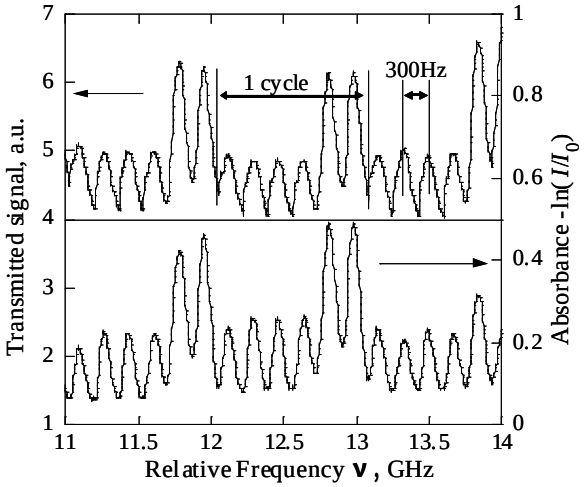

Fig. 15 Oscillation of the emission signal and absorbance.

The absorbance is composed of the optical path-integrated absorption coefficients, so the Abel inversion [30] is applied to each extracted local maximum and minimum points in order to obtain the spatially resolved absorption coefficients, assuming the axisymmetric distribution. As a result, the history of the number density at the center of IPG3 flow is obtained as shown in Fig. 16. Maximum number density is 5.1×10^{16} m^{-3}.To be combined with the result of LIF measurement, the time averaged number density is deduced as 3.1×10^{16} m^{-3}.

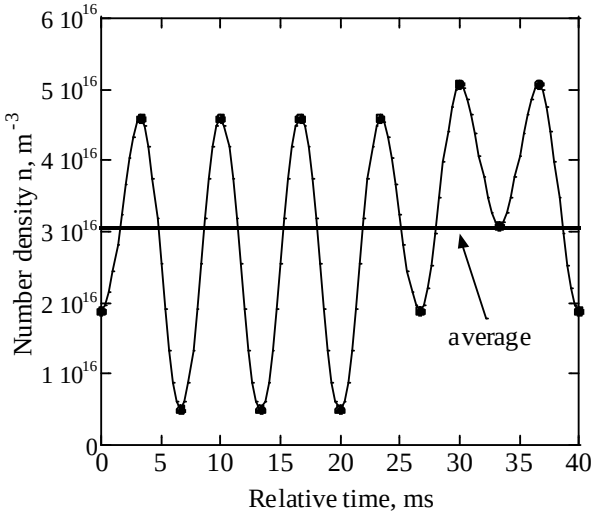

Fig. 16 History of the number density of the excited state atomic oxygen.

3.4.2. Population temperature

The population temperature T_{pop} defined by the ground state and 3s3S state is estimated by substituting n_g and n_{844} into the Boltzmann equation which is shown in Eq. (9). As a result, T_{pop} is obtained as 12000 K.

$$n_j = \frac{g_j}{g_i} n_i \exp(-\frac{\Delta E_{ij}}{k_B T_{pop}}) \tag{9}$$

Further n_{777} was estimated as 4.0×10^{17} m^{-3} [31]. So by substituting n_g and n_{777} into Eq. (9), T_{pop} defined by the ground state and 3s5S is estimated as 14000 K. This value shows a good agreement with the T_{pop} defined by the ground state and 3s3S.

T_{pop} of from 12000 K to 14000 K is reasonable as the electron temperature in the IPG3. So it is important to measure the axial distribution of T_{pop} and to know how T_{pop} decreases. And it is necessary to numerically simulate T_{pop} of the flow and verify the validity of the experimentally measured population temperature. Furthermore by building the CR model of atomic oxygen, the electron density and electron temperature can be obtained. This is important to figure out whether the distribution of the number density of each energy level follows the local thermo equilibrium.

3.5. Summary

The number density of the atomic oxygen in the metastable state 3s3S is measured by the laser absorption spectroscopy. And the time averaged number density is deduced as 3.1×10^{16} m^{-3}. By the combination of this result with the number density of the ground state atomic oxygen measured by

the laser induced fluorescence, the population temperature is obtained.

The population temperature defined by the ground state and 3s3S is estimated as 12000 K. The population temperature defined by the ground state and 3s5S is also estimated as 14000 K. These values show a good agreement. These results help to understand the plasma condition in detail with the measurement of the electron temperature or electron density.

Chapter 4. Effects of the mechanical vibration in the cavity enhanced absorption spectroscopy

As described in Chapter 1, in the application of CEAS to the wind tunnel measurements, there are some tasks. In this work the influence of the mechanical vibration to the optical cavity is experimentally studied.

4.1. Theory of the optical cavity

4.1.1. Without vibration

First the theory of optical cavity is explained. As explained in [32], some properties of optical cavity can be derived from the theory of Fabry Perot interferometer. The ratio of the transmitted intensity to the initial intensity is described as

$$\frac{I_t}{I_0} = \frac{1}{1 + \dfrac{4R\sin^2\left(k_0 nd\cos\theta_t\right)}{\left(1-R\right)^2}}. \tag{10}$$

Here R, k_0, n, d and θ_t are a reflectivity of the mirror, wave number, refractive index, cavity length, and angle of incident, respectively. This is known as an Airy function. Fig. 17 shows the normalized transmitted intensity as a function of the relative phase shift for R = 0.999, n = 1 and θ_t = 0. The full width at half maximum (FWHM) of the transmitted signal $\delta\omega$ is described as

$$\delta\omega = \frac{c}{2d}\frac{1-R}{\pi\sqrt{R}}. \tag{11}$$

The higher R is, the smaller $\delta\omega$ is. And $\delta\omega$ is in inverse proportion to d. In case that d is 1 m and R is 0.999, $\delta\omega$ is about 48 kHz and for R = 0.999 $\delta\omega$ is about 4.8 kHz. This is smaller than the FWHM of diode laser which is usually from 1 MHz to 300 kHz.

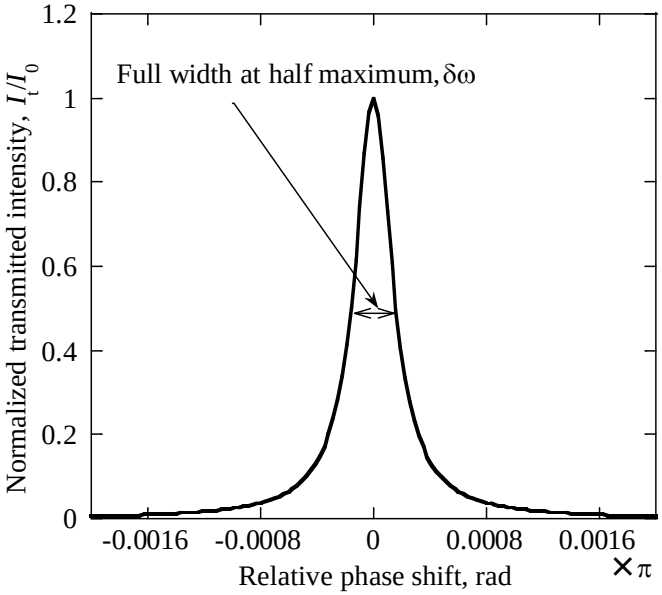

Fig. 17 Profile of the normalized transmitted intensity (R=0.999)

Equation (10) has a maximum value when

$$k_0 nd\cos\theta_t = m\pi\,. \tag{12}$$

Here m is an integer number. By transforming k_0 into frequency of the laser, the frequency at which the transmitted intensity has a maximum value is described as follows,

$$\nu = \frac{mc}{2nd\cos\theta_t}\,. \tag{13}$$

And now n and θ_t can be seen as unity and zero, respectively. The free spectral range (FRS) ν_{FSR} is defined as

$$\nu_{FRS} = \frac{c}{2d}\,. \tag{14}$$

The spectral resolution is determined by ν_{FSR}. In the application of CEAS to the wind tunnel measurements typically d is around 2 m, so ν_{FSR} is 74.9 MHz. This value is small enough to measure Doppler broadening of a few GHz. When the laser frequency is modulated, ν is a function of the time as follows,

$$\nu(t) = \nu_0 + u_L t\,. \tag{15}$$

In case that the laser is modulated by a ramp voltage, u_L can be written as

$$u_L = 2\Delta\nu_L f_L\,. \tag{16}$$

Here $\Delta\nu_L$ and f_L are the range of the laser modulation and the frequency of the laser modulation respectively. $\Delta\nu_L$ can be defined as a positive value for the increasing modulation of ν and a negative value for the decreasing modulation of ν. If $\Delta\nu_L$ and f_L are 20 GHz and 1 Hz respectively, the history of the normalized transmitted intensity is calculated as shown in Fig. 18.

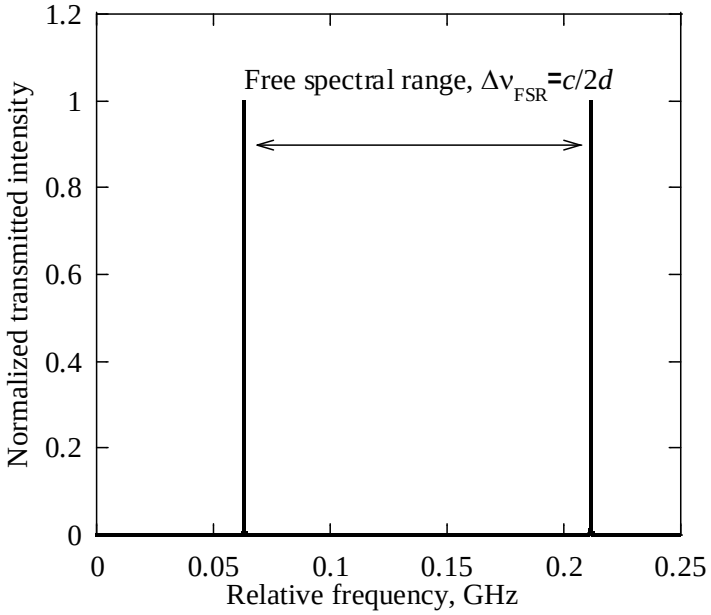

Fig. 18 Calculated normalized transmitted intensity as a function of the relative frequency of the laser (R =0.999, f_L=1Hz, $\Delta\nu$ = 20GHz, d =1 m)

4.1.2. With vibration

If there is a vibration in the direction of the laser path, d is a function of time. Here the vibration is described as the triangle waveform as

$$d(t) = d_0 + 4a_c f_c t \,. \tag{17}$$

Here a_c and f_c is the amplitude of vibration and frequency of vibration, respectively. Also here a_c can be defined as positive for increasing change of d and negative for decreasing change of d. Now it is assumed that at the time of t_0,

$$\nu(t_0)d(t_0) = \nu_0 d_0 \,. \tag{18}$$

Then after the time of Δt,

$$\nu(t_0 + \Delta t)d(t_0 + \Delta t) = (\nu_0 + 2\Delta\nu_L f_L \Delta t)(d_0 + 4a_c f_c \Delta t) \tag{19}$$

So the phase shift is

$$\Delta\nu d = \frac{2\pi}{c}(4\nu_0 a_c f_c + 2d_0 \Delta\nu_L f_L)\Delta t \,, \tag{20}$$

neglecting the term of squire of Δt. In this work ν_0, d_0 and $\Delta\nu_L$ are fixed. And the dependency of transmitted intensity profile on a_c, f_c, and f_L is discussed.

4.2. Vibration influence to the optical cavity

In the application of CEAS to the wind tunnel measurements there are many kinds of mechanical vibrations from the vacuum pump or experimental facilities and the superposition of all vibration makes the total influence to the optical cavity. The direction of such vibrations can be along three axes and are complicated. The optical cavity was built up at the arc wind tunnel of JAXA. The cavity length is 2 m. The influence of the vibration is classified into two types. One is the increase of the number of resonance $N_{\text{resonance}}$. And the other is the increase of the deviation of the transmitted intensity.

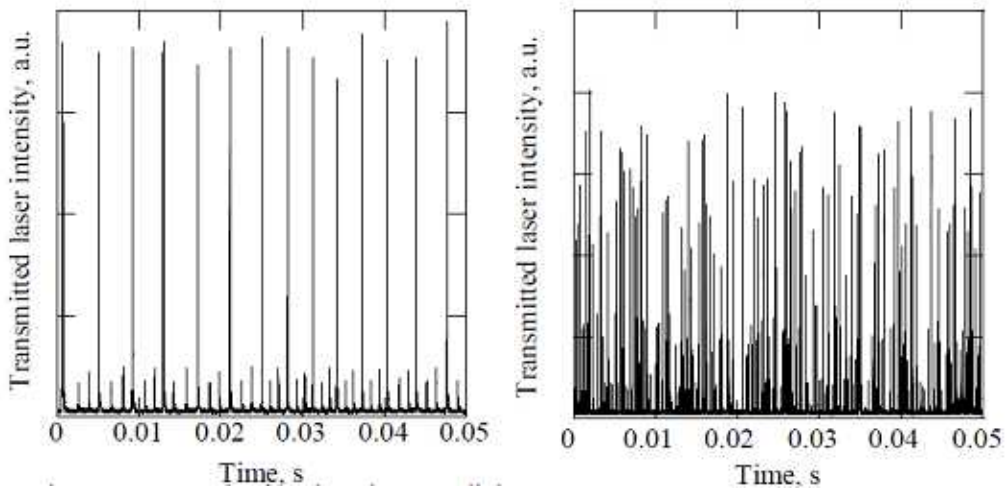

Fig. 19 Temporal transmitted laser intensity in the application to an arc wind tunnel of JAXA (left; without the operation of wind tunnel, right; with the operation of wind tunnel)

4.3. Experimental setup

The schematic overview of the experimental setup is shown in Fig. 20. As a light source, the same external cavity diode laser as used in Chapter 2 was used. The laser wavelength is from 768 to 788 nm and can be tuned 75 GHz (c.a. 0.15 nm). In this work $\Delta\nu_L$ was fixed at 20 GHz and f_L was from 0.25 to 100 Hz. The maximum value of f_L is limited by the ability of the piezoelectrical transducer mounted at the external cavity of the laser. And the laser was operated around 770 nm, which corresponds to 3.89 x 10^5 GHz. The laser power is 10mW. The optical cavity was built up by using the highly reflective mirrors (HR 820, Layer tec.) with a diameter of 1 inch and a radius of curvature of 1000 mm. A radius of curvature of the mirror is also important for the design of the optical cavity. The cavity length is 700 and 1100 mm, which corresponds to the free spectral range of 214 and 143 MHz. In order to simulate the vibration to the cavity one of the mirrors is mounted on a

piezoelectric translator, PZT (NF15AP25/M, Thorlab, Inc.) and the mirror is vibrated in the direction of the laser path. The amplitude of the vibration a_c is 2, 0.5, 0.25 and 0.05 μm. The frequency of the vibration f_c is up to 300 Hz. The transmitted signal is detected by a photo multiplier tube, PMT (H8249-200, HAMAMATSU) with a band pass filter (FB 780-10, Thorlab, Inc.). The data is recorded by a 14 bit digital oscilloscope (DL708E, Yokogawa, Co.) with a sampling rate which is high enough to record the very sharp transmitted signal. If there is a chamber inside the optical cavity, in order to minimize the intensity loss at the window of the chamber, the Brewster angle window is used. And the polarization of the laser has to be controlled. The detail of this scheme is described in [32].

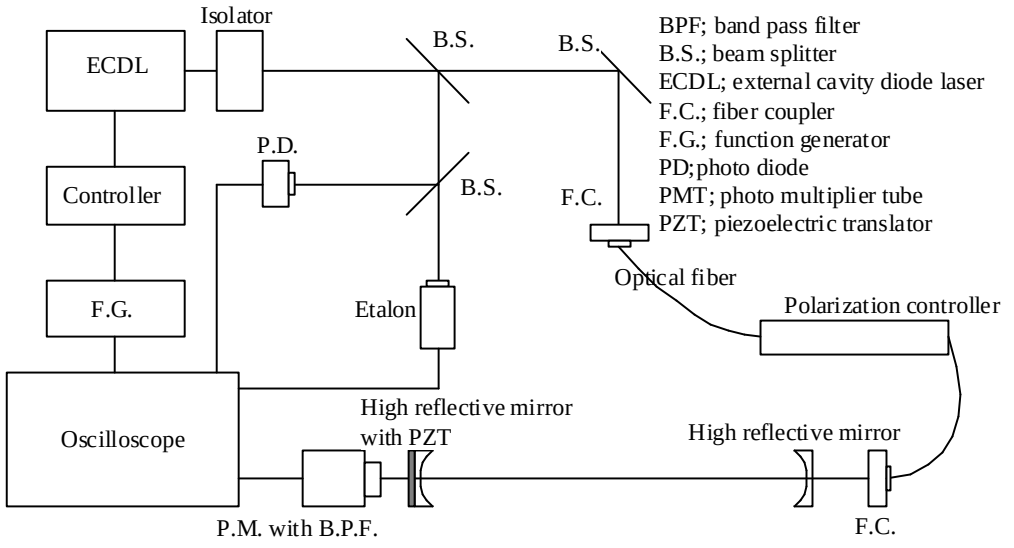

Fig. 20 Schematic of the experimental setup of CEAS

4.4. Results and discussions

Here simply the vibration in the direction of the optical path is simulated by the PZT since the change of the cavity length largely contributes to the change of the transmitted signal. Fig. 21 shows a typical transmitted signal without and with vibration. Also here the influences of the vibration are the increase of $N_{\text{resonance}}$ and the increase of the deviation of the data. The increase of $N_{\text{resonance}}$ is a good effect. The time interval of the each transmitted signal is shorter than that of the transmitted signal without vibration. So the time resolution and also spectral resolution are improved. But the increase of the deviation of data is a bad effect. In CEAS the transmitted signal I_t is fitted by a function to I_{fitted}. Then the absorption coefficient is obtained from the absorbance $-\ln(I_t/I_{\text{fitted}})$. So the sensitivity of CEAS is limited by $\Delta I_t/I_{\text{fitted}}$. If the $\Delta I_t/I_{\text{fitted}}$ is comparable to the fractional absorption, it is difficult to detect the weak absorption. So it is important to know $\Delta I_t/I_{\text{fitted}}$ and how to decrease it.

So here the influence of the vibration is evaluated by $N_{resonance}$ and ΔI_t.

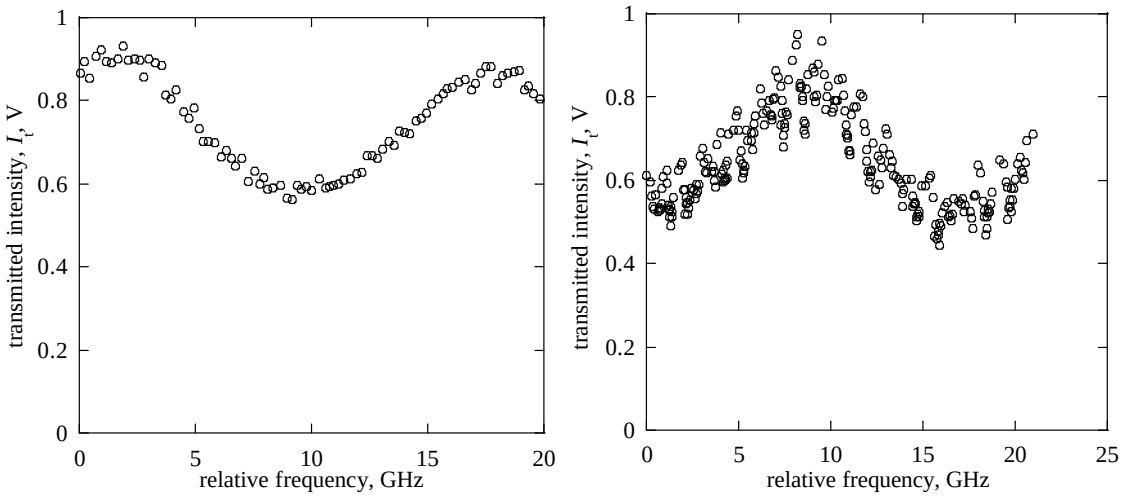

Fig. 21 Influence of the vibration of (f_L=1 Hz, and left one is without vibration, right one is with a_c = 4 μm and f_c = 13.2 Hz)

4.4.1. Dependency on a_c

Equation (20) can be rewritten as

$$\Delta kd = \frac{2\pi}{c} 2d_0 \Delta\nu_L f_L \left(\frac{2\nu_0 f_c}{d_0 \Delta\nu_L f_L} a_c + 1 \right) \Delta t \qquad (21)$$

To eliminate the influence of the vibration, the requirement for a_c is

$$a_c << \frac{d_0 \Delta\nu_L f_L}{2\nu_0 f_c} . \qquad (22)$$

The experimental results are shown in Fig. 22. Here d_0 = 0.7 m, $\Delta\nu_L$ = 20 GHz, f_L = 1 Hz, ν_0 = 3.89x10^5 GHz and f_c = 25 Hz. The right hand side of Eq. (21) is 700nm. As shown in Fig. 22, if a_c is smaller than 700 nm, the influence is small. In the application to the wind tunnel measurements d_0 is about 2 m. So in case of the low f_c, it is not difficult to keep the cavity length stable to avoid the influence of the vibration. For example if d_0 = 2 m, $\Delta\nu_L$ = 20 GHz, f_L/ f_c = 1 and ν_0 = 3.89x10^5 GHz, the right-hand side value is 50 μm.

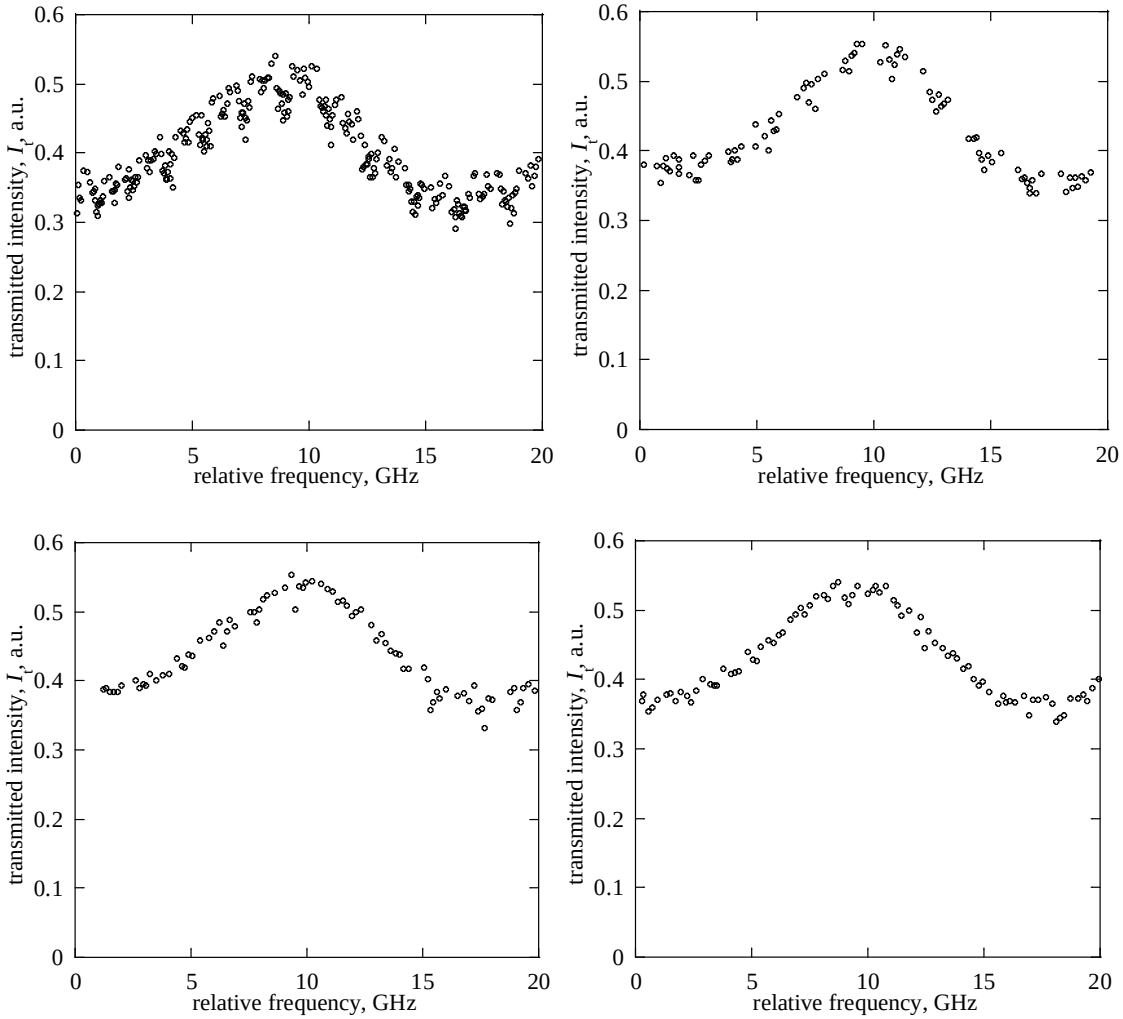

Fig. 22 Transmitted signal with different a_c (upper left; 4 μm, upper right; 1 μm, bottom left; 0.5 μm and bottom right; 0.1 μm), and f_c is 25 Hz f_L is 1 Hz, d is 0.7 m.

4.4.2. Dependency on f_L

The dependency of transmitted intensity profile on f_L is evaluated. Here a_c and d are 4 μm and 0.7 m. Fig. 23 shows the transmitted signal for two different f_L and f_c is fixed at 50 Hz. At the slower modulation of the laser frequency the number of resonance per laser frequency range of 1 GHz $N_{resonance}$ is large. And also the deviation in the data is large.

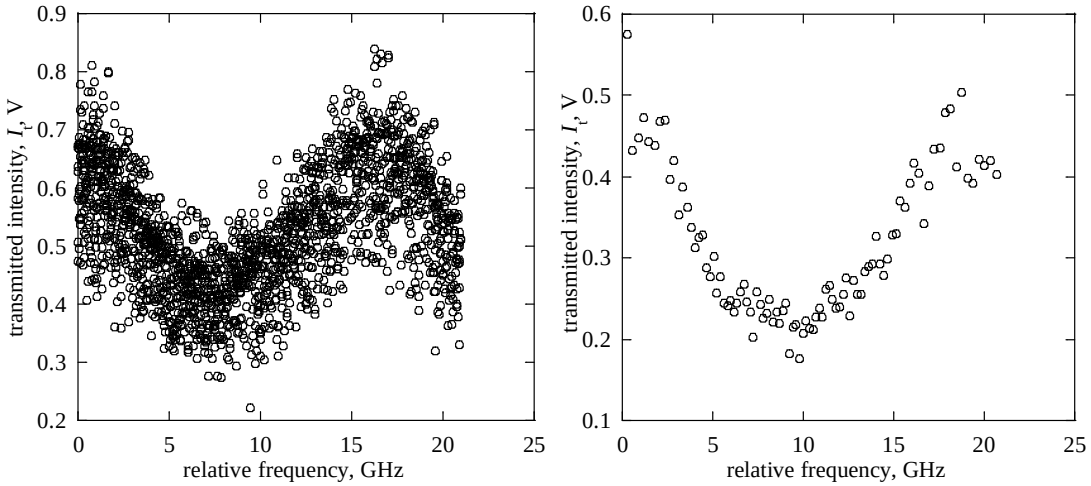

Fig. 23 Transmitted intensity for f_L=0.25 Hz (left) and 25 Hz (right)

The relationship between $N_{resonance}$ and f_L is shown in Fig. 24. The slower the laser modulation speed is the larger $N_{resonance}$ is observed. And at f_L which is higher than a certain value $N_{resonace}$ converges to the value of 4.7 (= 1GHz / $\Delta\nu_{FSR}$) for any frequency of vibrations.

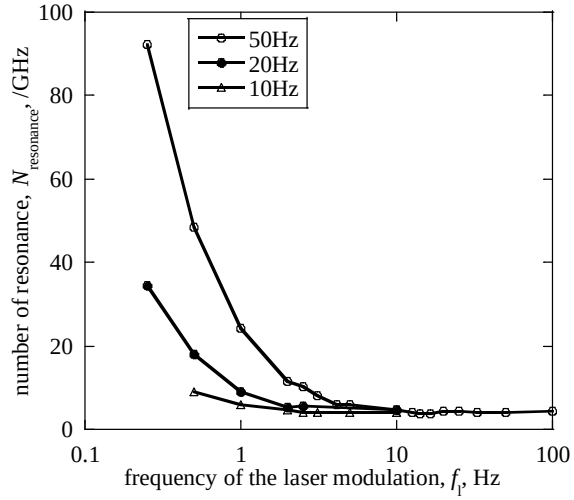

Fig. 24 Relationship between $N_{resonance}$ and f_L for f_c = 50, 20 and 10 Hz

The ratio of f_L to f_c from which the influence of the vibration decreases can be estimated as follows. From Eq. (20), the requirement to eliminate the influence of the vibration is as

$$f_L >> \frac{2\nu_0 a_c}{d_0 \Delta\nu_L} f_c \,. \tag{23}$$

Here $\nu_0 = c/\lambda_0 = 3.89\text{x}10^5$ GHz, $a_c = 2\text{x}10^{-6}$ m, $d_0 = 0.7$ m and $\Delta\nu_L = 20$ GHz, so the right-hand side is 0.11 x f_c.

4.4.3. Requirements for the measurement with a high speed modulation of the laser

If f_L is high enough it is possible to eliminate the influence of the vibration. But the higher f_L is, the higher sampling rate is desired. According to Eqs. (11) and (16), the time the laser takes to sweep $\delta\omega$ is

$$t_{\delta\omega} = \frac{\delta\omega}{u_L} = \frac{c}{4d}\frac{1-R}{\pi\sqrt{R}}\frac{f_L}{\Delta\nu_L} \tag{24}$$

Considering the measurement of the atomic oxygen or nitrogen in the arc heated or inductively heated air flow, which translational temperature is from 1000 to 5000 K, it is necessary to set $\Delta\nu_L$ about 20 GHz. Typically R and d are 0.9999 and 2 m respectively. If f_L is higher than 100 Hz, $t_{\delta\omega}$ is less than 1ns. In order to record ten samples during the time of $t_{\delta\omega}$ for f_L = 100 Hz, the sampling rate of 17 GS/s is necessary and the rise time of PMT should be less than 1 ns.

4.4.4. Dependency on f_c

In CEAS the transmitted signal I_t is fitted by a function as shown in Fig. 25. Here the fitting function is a six order polynominal. As noted before, the deviation of I_t from I_{fitted} determines the sensitivity limit of CEAS. In Fig. 25, the average of $\Delta I_t/I_{fitted}$ is 0.017. So it can be said that the sensitivity limit is the fractional absorption of about 0.017.

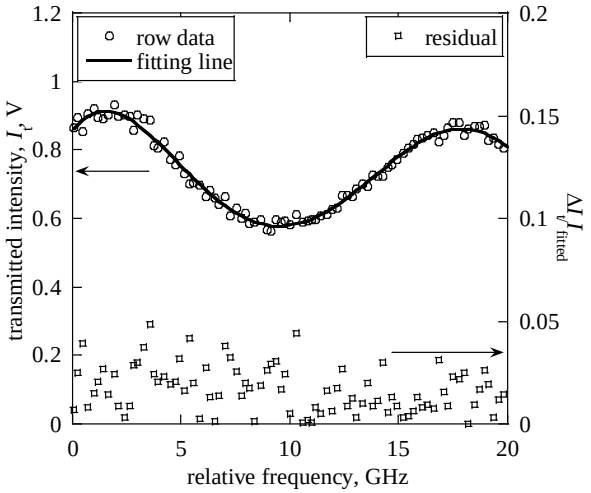

Fig. 25 Transmitted signal and fitting line with the residual (f_c = 1.3 Hz, d_0 = 0.7 m, f_L = 1 Hz)

At a certain frequency of the vibration the transmitted signal shows the large $\Delta I_t/I_{fitted}$ as shown in Fig. 26.

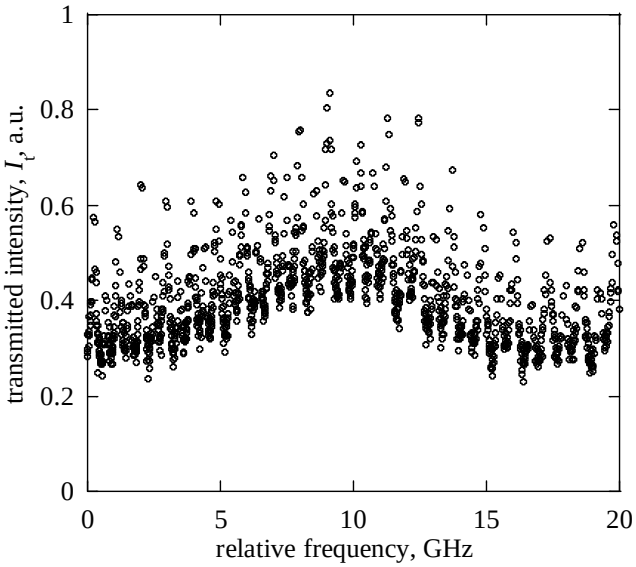

Fig. 26 Transmitted signal which shows the large deviation (f_L = 1 Hz, f_c=13.6Hz, d=0.7 and a_c = 4 μm)

The relationship between $\Delta I_t/I_{fitted}$ and f_c is shown in Fig. 27. Here a_c, f_L and d are 4 μm, 1 Hz and 0.7 m, respectively.

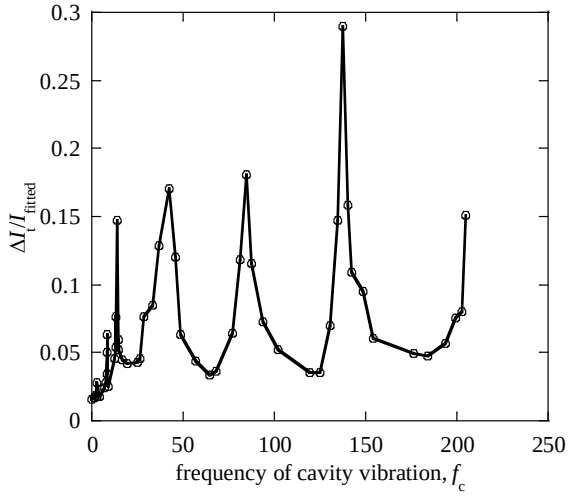

Fig. 27 Relationship between $\Delta I/I_{fitted}$ and f_c

The periodical behavior of $\Delta I_t/I_{fitted}$ can be seen in Fig. 27. As shown in Eq. (20), if the following requirement is satisfied, the transmitted signal is dominated by f_c.

$$f_c >> \frac{d_0 \Delta \nu_L f_L}{2\nu_0 a_c}. \tag{25}$$

In this case the right hand side is 10 Hz. So in the region of f_c higher than 50 or 100 Hz, it might be said that only f_c contributes to the change of the transmitted signal. However, according to Eq. (10), the transmitted intensity doesn't vary along with d. The length of the optical cavity contributes only to the phase shift theoretically. So the deeper insight is needed to understand the reason why the large deviation of the transmitted laser intensity exits at the certain frequency of the vibration.

4.5. Summary

The influence of the mechanical vibration is studied experimentally.

1) As to the dependency of the amplitude of the vibration, in case of d_0 = 2 m, $\Delta\nu_L$ = 20 GHz, f_L/f_c = 1 and $\nu_0 = 3.89\text{x}10^5$ GHz, by keeping the optical cavity stable in the range of less than 50 μm, the influence of the vibration can be avoided.

2) As to the dependency of the frequency of the laser modulation, it is confirmed that by setting the f_L high enough, the influence can be decreased. But in the application of the high frequency laser modulation, it is necessary to use a high sampling rate data acquisition system.

3) As to the dependency of the frequency of the vibration, the large deviation of the transmitted intensity is observed at a certain frequency. To make it clear it is necessary to investigate more deeply.

Chapter 5. Conclusions

The novel measurement method to estimate the specific heat ratio by the combination of the laser absorption spectroscopy with the pitot probe measurement is developed in the arc heater wind tunnel measurement. And the accuracy of this method is deduced as 3.2 %.

The laser absorption spectroscopy was applied to the quasi stationary plasma flow measurement. By the combination of the laser absorption spectroscopy with the laser induced fluorescence, the population temperature of the inductively heated plasma wind tunnel flow is obtained as 12000 K.

The experimental study of the influence of the mechanical vibration to the optical cavity is experimentally studied. And the dependency of the amplitude of the vibration and frequency of the laser modulation and frequency of the vibration is described. For the dependency of the frequency of the vibration, it is necessary to investigate in detail.

Chapter 6. References

[1] Kawaguchi, J., Fujiwara, A., and Sawai, S., Acta Astronautica, **38** (1996), 87-101

[2] Scott, C. D., AIAA paper 80-1477, 1980

[3] Liu, I. D., and Steinberg, M., J.Q.S.R.T., **8** (1968), 161-169

[4] Nozawa, S., Symposium on Flight Mechanics and Astrodynamics, 2008

[5] Kobayashi, Y., Symposium on Flight Mechanics and Astrodynamics, 2008

[6] Inoue, T., Doctor thesis, The University of Tokyo, 2007

[7] Matsui, M., Doctor thesis, The University of Tokyo, 2005

[8] Anthony, A., Boiarski, Aerospace research laboratories, ARL 72-0126, 1972

[9] Loele, S., Auweter-Kurtz, M., Pidan, S., and Herdrich, G., AIAA Paper 2004-2596, 2004

[10] Kim, S., Doctor thesis, Stanford University, 2004

[11] Zaatar, Y., Bechara, J., Khoury, A., Zaouk, D. and Charles, J.-P., Appl. Energy, **65** (2000), 107-113

[12] Mark, G Allen, Mea. Sci. Technol. **9** (1998), 545-562

[13] Hanson, R. K., Kuntz, P. A. and Kruger, C. H., Appl. Opt., **16** (1977), 2045-2048

[14] Hirmke, J., Schwarz, S., Hempel, F., Stancu, G. D., Roepcke, J. And Rosiwal, S., Journal of Superhard Materials, **29** (2007), 133-137

[15] Nagali, V., Herbon, J. T., Horning, D. C., Davidson, D. F. and Hanson, R. K., Appl. Opt. **38** (1999), 6942-6950

[16] Matsui, M., Ikemoto, T., Takayanagi, H., Komurasaki, K. and Arakawa, Y., Journal of Thermophysics and Heat Transfer, **21** (2007), 247-249

[17] Matsui, M., Komurasaki, K., Herdrich, G. and Auweter-Krutz, M., J. AIAA **43** (2005), 2060-2064

[18] Mazurenka, M. and Orr-Ewing, A.J. and Peverall, R. and Ritchie, G.A.D., Annual Reports Section" C"(Physical Chemistry), 101 (2005), 100-142

[19] O'keefe, A., Deacon, David, A. G., Rev. Sci. Instrum., **59** (1988), 2544-2551

[20] Meijer, G., Boogaarts, M., Jongma, R. T., Parker, D. H. Chem. Phys. Lett., **217** (1994), 112 - 116

[21] Hodges, J. T., Looney J. P., and Zee R. D., Appl. Opt., **35** (1996), 4112-4116

[22] Martin, J., Paidus, B. A., Zalicki, P., Wahl, E. H., Owano, T.G., Harris, J. S., Kruger, C. H., and Zare, R. N., Chem. Phys. Lett. **258** (1996), 63-70

[23] Romanini, D., Kachanov, A. A., Sadeghi, N., and Stoeckel, F., Chem. Phys. Lett., **264** (1997), 316-322

[24] Lehmann, K. K., Romanini, D., J. Chem. Phys. **105** (1996), 10263-10277

[25] Engeln, R., Berden, G., Peeters, R., and Meijer, G., Rev. Sci. Instr., **69** (1998), 3763-3769

[26] A. O'Keefe, Chem. Phys. Lett., **293** (1998), 331-336

[27] Y. He, Chem. Phys. Lett., **289** (1998), 527

[28] Herdrich, G., Auweter-Krutz, M., Laux, T. And Winter, M., Journal of Thermophysics and Heat transfer, **16** (2002), 440-449

[29] Loele, S., Eichhorn, C., Steinbeck, A., Lein, S., Herdrich, G., Roeser, H. P. and Auweter-Krutz, M., Appl. Opt., **47** (2008), 1837-1845

[30] Choi, B. S. and Kim, H., Appl. Spectrosc., **36** (1982), 77-74

[31] Matsui, M., Herdrich, G., Auweter-Krutz, M. and Komurasaki, K., AIAA paper 2003-3898, 2003

[32] Takayanagi, H., Doctor thesis, The University of Tokyo, 2007